JOURNAL OF PROPULSION AND POWER
Vol. 21, No. 3, May–June 2005

Test Rig for Evaluating Active Turbine Blade Tip Clearance Control Concepts

Scott B. Lattime* and Bruce M. Steinetz†
NASA Glenn Research Center, Cleveland, Ohio 44135
and
Malcolm G. Robbie‡
Analex Corporation, Cleveland, Ohio 44142

Improved blade tip sealing in the high-pressure compressor and high-pressure turbine can provide dramatic improvements in specific fuel consumption, time on wing, compressor stall margin, and engine efficiency, as well as increased payload and mission range capabilities of both military and commercial gas-turbine engines. The design of a first-generation mechanically actuated active clearance control system for turbine blade tip clearance management is presented, along with the design of a bench top test rig in which the system is to be evaluated. The active clearance control system utilizes mechanically actuated seal carrier segments and clearance measurement feedback to provide fast and precise active clearance control throughout engine operation. The purpose of this active clearance control system is to improve on current case cooling methods. These systems have relatively slow response and do not use clearance measurement, thereby forcing cold-build clearances to set the minimum clearances at extreme operating conditions and not allowing cruise clearances to be minimized due to the possibility of throttle transients. The test rig will simulate proper seal carrier pressure and temperature loading, as well as the magnitudes and rates of blade tip clearance changes of an actual gas-turbine engine. The results of these evaluations will be presented in future works.

Nomenclature

A	=	cross-sectional area of rod, in.^{2} (mm^2)
A^*	=	cross-sectional area under choked flow conditions, in.^{2} (mm^2)
C	=	Larson–Miller constant, 20
C_L	=	flow loss coefficient
C_p	=	specific heat of air, Btu/lbm · °F (J/kg · K)
f	=	friction factor
h	=	clearance, in. (mm)
k	=	thermal conductivity, Btu/h · ft · °F (W/m · K)
L	=	length of rod, in. (mm)
M	=	Mach number
M_1	=	inlet Mach number
M_2	=	outlet Mach number
$\dot{m}$	=	mass flow of air, lbm/h (kg/s)
P	=	Larson–Miller parameter
P_3	=	air pressure exiting high-pressure compressor, psi (kPa)
p_1	=	inlet pressure, psi (kPa)
p_2	=	outlet pressure, psi (kPa)
q_{cond}	=	heat conducted through rod, Btu/h (W)
q_{conv}	=	heat convected by mass flow, Btu/h (W)
R	=	gas constant, Btu/lbm · R (kJ/kg · K)
Re	=	Reynolds number
T	=	temperature, R (K)
T_c	=	temperature of rod (cool end), °F (°C)
T_h	=	temperature of rod (hot end), °F (°C)
T_i	=	temperature of air in, °F (°C)
T_o	=	temperature of air out, °F (°C)
T_3	=	air temperature exiting high-pressure compressor, °F (°C)
t	=	time to produce creep condition of interest, for example, 0.5% creep strain, h
u	=	air velocity, ft/s (m/s)
γ	=	specific heat ratio
λ	=	Pressure ratio
μ	=	dynamic viscosity, lbm/ft · s (N · s/m^2)
ρ	=	density, lbm/ft^3 (kg/m^3)

Introduction

GAS path sealing continues to be an important component with regard to improving turbine engine efficiency and operation. Blade tip sealing has remained a challenging problem since the development of the gas-turbine engine. Environmental conditions at the tip seal location include gas temperatures up to 2500°F (1371°C), surface speeds up to 1500 ft/s (457 m/s), as well as unburned jet fuel and contaminants (dirt, sand, etc.) that make for very challenging surroundings for a controllable seal design. In addition to the extreme operating environment, these conditions change due to engine operation and environmental conditions outside the engine, which, in turn, act to vary the clearance between the rotating blade tips and the surrounding static casing (shroud).

Improved blade tip sealing in both the high-pressure compressor (HPC) and high-pressure turbine (HPT) can provide dramatic improvements in specific fuel consumption (SFC), compressor stall margin, and engine efficiency, as well as increased payload and mission range capabilities. Improved clearance management, especially in the HPT, can dramatically improve engine service life or time on wing (TOW). Maintenance costs for major overhauls

Presented as Paper 2003-4700 at the AIAA/ASME/SAE/ASEE 39th Joint Propulsion Conference, Huntsville, AL, 21–24 July 2003; received 31 December 2003; revision received 2 September 2004; accepted for publication 10 October 2004.

*Senior Researcher, Mechanical Components, NASA Glenn Research Center, Mail Stop 23-3, 21000 Brookpark Road. Member AIAA.

†Senior Research Engineer, Mechanical Components, NASA Glenn Research Center, Mail Stop 23-3, 21000 Brookpark Road. Associate Fellow AIAA.

‡Senior Design Engineer, NASA Glenn Research Center, Mail Stop 301-2, 21000 Brookpark Road.

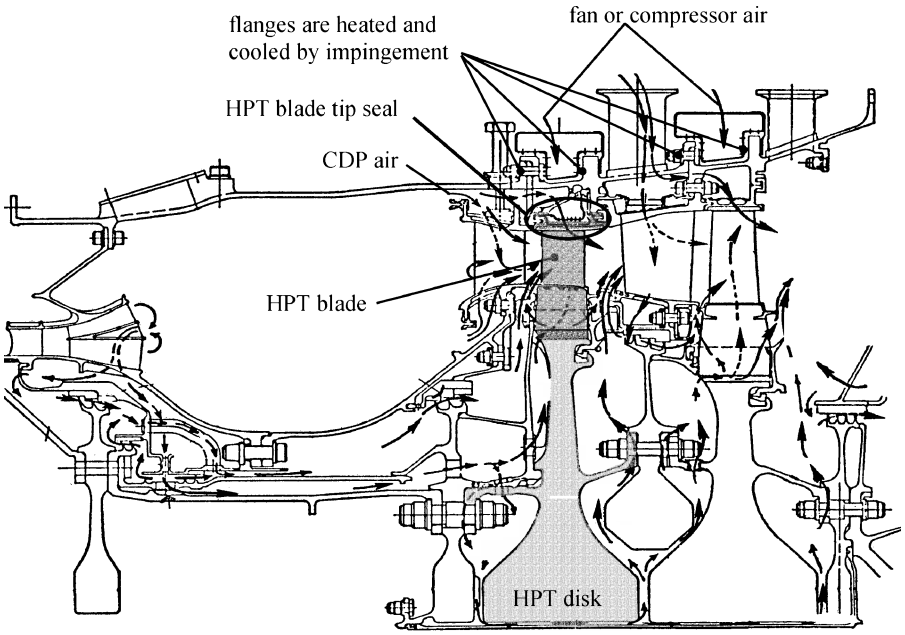

Fig. 1 HPT blade tip seal location in a modern gas-turbine engine.[1]

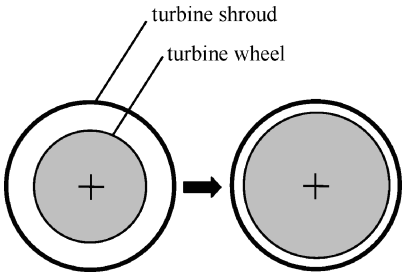

Fig. 2 Axisymmetric clearance change.

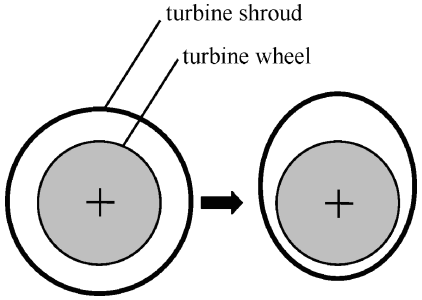

Fig. 3 Asymmetric clearance change.

of today's large commercial gas-turbine engines can easily exceed $1 million.

Background

Figure 1 shows the HPT blade tip seal location in a modern gas-turbine engine.[1] Figure 1 shows a cross section of the combustor and two-stage HPT. The turbine disk, blade, and tip seal of the first-stage turbine are labeled. Blade tip or outer air seals line the inside of the stationary case, forming a shroud around the rotating blades, limiting the gas that spills over the tips. Blade tip clearance varies over the operating points of the engine, for example, ground idle, takeoff, cruise, deceleration, etc., as well as over the cycle life of the engine. These clearance variations are due to a number of loads on both static and rotating parts and wear of these parts.

Load mechanisms can be separated into two categories, namely, engine (power-induced) loads and flight loads. Engine loads include centrifugal, thermal, internal engine pressure, and thrust loads. Flight loads include inertial (gravitational), aerodynamic (external pressure), and gyroscopic loads. Engine loads can produce both axisymmetric and asymmetric clearance changes. (Figs. 2 and 3.) Flight loads produce asymmetric clearance changes. Load mechanisms generally act to alter blade tip clearance temporarily, whereas wear mechanisms permanently change tip clearance.

Wear mechanisms of blade tip seals can generally be separated into two categories, namely, rubbing (blade incursion), and erosion. Blade rubs and erosion are expected to occur throughout the service life of an engine. Engine build clearances are, in fact, sometimes chosen to operate line-to-line at extreme operating conditions, for example, takeoff and reacceleration. In this case, manufacturers set cold-build clearances such that during the engine green state ("run-in") the blades will lightly rub the seal shrouds, thereby achieving tight clearances and mitigating the effects of manufacturing tolerance stack-up. Rubs can also contribute to accelerating the effects of both erosion and thermal fatigue by wearing protective coatings, for example, thermal barrier coatings, or distorting cooling passages of the blade tips during an incursion event. Lattime and Steinetz provided a comprehensive review on the mechanisms of tip clearance variation, their effects in gas-turbine engines, methods of controlling tip clearance, and the benefits associated with reducing tip clearance.[2] A review of some of the benefits of reduced tip clearance is presented here.

Blade tip clearance directly influences gas-turbine performance, efficiency, and life. Reducing air leakage over the blade tips increases turbine efficiency and permits the engine to meet performance and thrust goals with less fuel burn and lower rotor inlet temperatures. Running the turbine at lower temperatures increases the cycle life of hot section components, which, in turn, increases engine service life (TOW) by increasing the time between overhauls.

Fuel Savings

Engine SFC and exhaust gas temperature (EGT) are directly related to HPT blade tip clearances. Wiseman and Guo[3] indicate that for every 0.001-in. (0.025-mm) increase in HPT tip clearance, SFC increases approximately 0.1%, whereas EGT increases 1°C. Thus, a 0.010-in. (0.254-mm) HPT tip clearance decrease would roughly produce a 1% decrease in SFC and a 10°C decrease in EGT. Military engines generally show slightly greater HPT tip clearance influence

on SFC and EGT due to their higher operating speeds and temperatures compared to large commercial engines. Improvements of this magnitude would produce huge savings in annual fuel and engine maintenance costs. Lattime and Steinetz projected cost savings for U.S. carrier's fuel usage of over $160 million for the year 2003 alone, due only to a modest 1% reduction in SFC, based on 2001 average fuel prices.[2]

Reduced Emissions

Reducing fuel consumption also reduces aeroengine total emissions. The Rocky Mountain Institute estimates that Americans alone now fly 764 million trips per year (2.85 airline trips per person).[4] The energy used by commercial aircraft has nearly doubled over the last three decades. The increased fuel consumption accounts for 13% of the total transportation sector emissions of carbon dioxide (CO_2). Modern aeroengine emissions are made up of over 71% CO_2 with about 28% water (H_2O) and 0.3% nitrogen oxide (NO_2), along with trace amounts of carbon monoxide (CO), sulfur dioxide (SO_2), etc. Air transport accounts for 2.5% [$6E + 8$ tons ($5.44E + 11$ kg)] of the world's CO_2 production.[5] Clearly, a reduction in fuel burn will significantly reduce aeroengine emissions.

Extended Service Life

Current large commercial engines have life cycles (time between overhauls) that vary significantly, for example, 3000–10,000 cycles. Their cycle lives are basically determined by how long they retain a positive EGT margin. New engines or newly overhauled engines are shipped with a certain cold-build clearance. This clearance increases with time due primarily to rubs early in the engine's life.[6] Martin reported a 1% loss estimate in engine performance due to clearance changes that occurs during the production flight-test acceptance profile.[7] As the engine operating clearances increase, the engine must work harder (hotter) to produce the same work and is, therefore, less efficient. This increase in operating temperature, particularly takeoff EGT, further promotes the degradation of hot section components due to thermal fatigue. Retaining engine takeoff EGT margin by maintaining tight tip clearances and either eliminating rubs or compensating for them can dramatically increase engine cycle life. This would lead to considerable savings in engine maintenance costs over a period of years due to the significant costs of engine overhauls.

Objectives

This work is part of a larger research effort to develop viable mechanical concepts for active clearance control (ACC) systems for use in the HPT section of large commercial aircraft to improve on the case-cooling methods employed today. The objective of this work is to present the development of a test rig for the evaluation of ACC system concepts that are currently being developed at the NASA Glenn Research Center. The design of a first-generation mechanical ACC system that utilizes independent hydraulic actuators will be presented in conjunction with the test rig design. The test rig will be used to analyze the ability of various actuator concepts to control the positioning of a segmented shroud seal support structure under properly simulated HPT temperature and pressure conditions with the required system response rate and accuracy.

Rig Design Overview

The design of a system to manage blade tip clearance is not a new topic. As Lattime and Steinetz reported in their review on clearance control systems, well over 100 patents exist in the United States alone pertaining to blade tip clearance control.[2] However, the authors have found virtually no published experimental results for these patented systems. The authors of this work have focused their efforts on designing mechanical ACC systems that articulate the seal shroud via mechanical linkages connected to actuators that reside outside of the extreme environment of the HPT. The authors opted for this style of design due to a lack of high-temperature/low-profile actuators that are presently available and that the system is to function in a large, commercial, axial-flow HPT. Radial compressor and turbine designs may encounter less risk in an ACC system that functions in the axial direction along the rotor shaft. Obviously, penetration through the case requires secondary seals, but the authors felt this tradeoff to be a more viable alternative than designing an actuation system that functions inside the HPT case. Leakage levels for the secondary seals have been determined to be small, as will be discussed in a later section.

The rig design was focused on simulating the environment surrounding the backsides of the seal segments. As such, the design was concentrated on simulating the temperature and pressure conditions that exist on the backsides of the seal segments, without the need for a rotating turbine. This greatly simplified the rig design. The authors plan to assess the response of the ACC system to the effects of a turbine wheel, that is, rapid clearance closures due to mechanical and thermal loads, by simulating closures electronically, as will be discussed later.

Rig Specifications

Specifications for the rig were chosen to simulate closely the environment (temperature and pressure) and operating requirements (displacement rate and magnitude) of large commercial engines.

Temperature and Pressure

The backside of the HPT shroud (blade outer air seal) is generally cooled with compressor discharge air {T_3 air: [1200–1300°F, (649–704°C)]}. This cooling is necessary for the shroud segments to survive the 2500°F (1371°C) and higher rotor inlet gas temperatures. The cooling air is also used to purge the leading and trailing edges of the shroud segments to provide a positive backflow margin from the hot rotor inlet flow. This cooling flow is shown in Fig. 4 for the first-stage shroud of a two-stage HPT. The pressures surrounding the shroud segment can be expressed as a function of the compressor discharge pressure (CDP). Flowpath pressure adjacent to the HPT shroud varies axially due to the work extracted by the turbine blades. For large commercial engines, the pressure of the cooling air behind the shroud is about 60 to 80% of CDP. Pressure in the tip clearance region varies axially from the leading to the trailing edge of the shroud from about 70 to 30% of CDP, respectively. To maintain a positive backflow margin from the rotor inlet air, the cooling pressure on the backside of the shroud must always be higher than the rotor inlet side. The radial pressure difference across the shroud creates a load inward to the shaft centerline. A resultant moment also exists on the shroud that is created by the nonuniform axial pressure distribution. CDP is highest during maximum thrust events such as takeoff and reacceleration. For large commercial engines, this translates to a maximum cooling air pressure differential of up to 150 psi (1034 kPa) across the shroud. Test rig components were designed to accommodate the aforementioned temperature and pressure magnitudes. However, the test rig will not simulate an axially varying pressure distribution across the seal carriers.

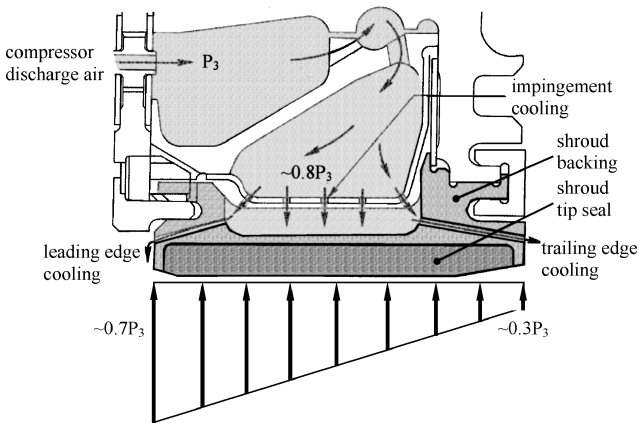

Fig. 4 Axial pressure distribution across HPT blade tip seal cross section.

Actuation Range and Rate

The largest HPT tip clearance variations, as discussed by Lattime and Steinetz, are due to centrifugal growth of the rotor during takeoff and reacceleration conditions.[2] Maximum tip clearance changes due to axisymmetric and asymmetric loads on the rotor, and stator components are on the order of 0.050 in. (1.27 mm). The Federal Aviation Administration requires that gas-turbine engines have the ability to reach 95% rated takeoff power from flight idle (or from 15% rated takeoff power) in 5.0 s (Ref. 8). In general, this requirement sets a limiting case of maximum displacement and minimum response time for actuation systems to be used as ACC. Given a maximum clearance change of 0.050 in. (1.27 mm), this would require actuation systems that can provide radial clearance change on the order of 0.010 in./s (0.254 mm/s). These response rates exclude faster dynamic clearance changes, that is, once per revolution events, that are beyond the scope of this effort.

Rig Design Criteria: Creep Life

The substantial diameter of the segmented shroud structure [∼20 in. (508 mm)], even under moderate pressures [∼120 psi (827 kPa)], gives rise to significant loads and, hence, stresses, to which the actuation system and components must react. These stresses, coupled with high temperatures [1200–1300°F (649–704°C)], can significantly reduce component cycle life due to creep. Managing these stresses with adequate materials and geometry to improve component cycle life was a driving factor in the rig component design. The authors utilized Larson–Miller parameter data for a variety of high-temperature super alloys to design components to achieve a desired minimum cycle life.

The Larson–Miller theory correlates the results of short-term elevated temperature material performance testing to long-term performance at more moderate temperatures. For each combination of material and stress level, the Larson–Miller theory relates a unique value of a parameter P to temperature and creep life by (see Ref. 9)

$$P = T(C + \log t) \tag{1}$$

Thus, for a specified creep life and temperature, a properly suited material and maximum stress can be graphically determined, provided that the Larson–Miller parameter data exist. The authors chose Inconel 718 as the material for most of the hot section components. These components were designed for less than 0.5% creep strain, resulting in a 15-ksi (103-MPa) limiting stress. This stress level corresponds to over 100,000 h life at 1300°F (704°C) and approximately 300 h life at 1500°F (816°C).

Test Rig and Support Systems

The test rig housing and main components are shown in Figs. 5–7. Figure 5 shows the outside of the housing, whereas Figs. 6 and 7 show the inside of the housing and the major components of the rig. The test rig comprises six main components: the housing, the radiant heater, the pressurized chamber, the seal carrier assembly, the actuator rod assemblies, and the hydraulic actuators.

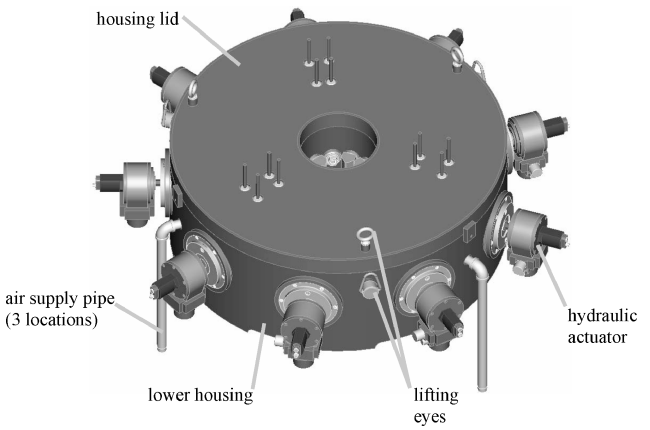

Fig. 5 ACC test rig.

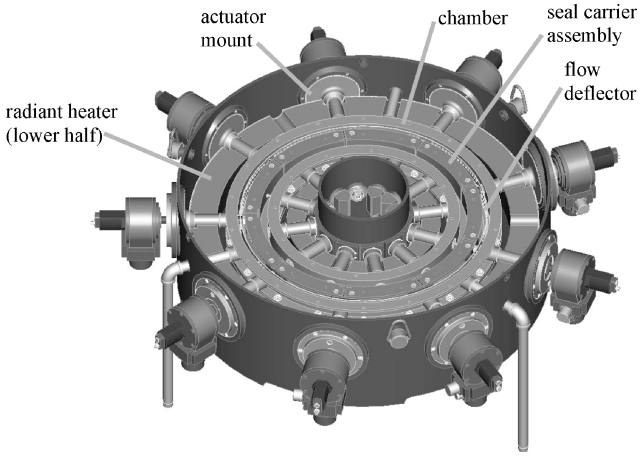

Fig. 6 ACC test rig with housing lid and chamber cover plate removed.

At the heart of the rig is a segmented shroud structure (seal carrier) that would structurally support the tip seal shroud segments in the engine. Radial movement of the seal carriers controls the effective position/diameter of the seal shroud segments, thereby controlling blade tip clearance. The carrier segments are connected to independent hydraulic actuators through an actuator rod assembly as shown in Figs. 6 and 7. The foot of the actuator rod assembly positions the carrier segments in the radial direction, while allowing relative circumferential movement or dilation of the seal carrier segments through a pinned and slotted arrangement as shown in Figs. 7 and 8.

The rig housing consists of two concentric cylinders that form an annular cavity. An annular radiant heater made of upper and lower halves surrounds the segmented seal carrier structure to simulate the HPT tip seal backside temperature environment. A pressurized chamber encloses the carrier segments inside the annular heater through which heated pressurized air is supplied to simulate the cooling/purge air pressure on the seal backsides. Heated air enters the chamber via three pipes that are fed from a manifold at the air heater exhaust through radial inlet ports as shown in Figs. 6 and 7. The flow is directed circumferentially around the outer chamber wall by a flow deflector that has a series of radial holes positioned about its circumference, except at the inlet positions. Air that escapes over and between the carrier segments is vented out of the rig through a number of exhaust pipes that protrude radially along the inner chamber wall. The number and inner diameter of exhaust pipes were chosen to eliminate the possibility of backpressure at the exhaust ports. The pressurized air is sealed along the sides of the seal carrier segments by contacting face seals that are energized via metal E seals embedded in the upper and lower chamber plates. The joints between adjoining carrier segments are sealed with thin metal flexures. A series of radial tubes projecting outward from the chamber's inner and outer side walls serve as supports, air supply and exhaust ports, probe fixtures, and the actuator rod guides. The chamber functions to support and align the carrier segments and actuator rods, as well as to house instrumentation and to seal the pressurized air from the radiant heater, which is not designed to carry any pressure loading.

High-temperature proximity probes measure the radial displacement of the seal carriers at various circumferential locations. These measurements provide direct feedback control to the independent actuators and allow the desired radial position (clearance) to be set. The direct feedback control system allows for simulation of realistic transient tip clearance changes in lieu of a rotating turbine wheel. Superimposing a mission-clearance profile over the actual clearance measurement input to the actuator controllers will allow researchers to assess the system's response to the most dramatic transient events, such as mechanical and thermal loading of the rotor during takeoff and reacceleration.

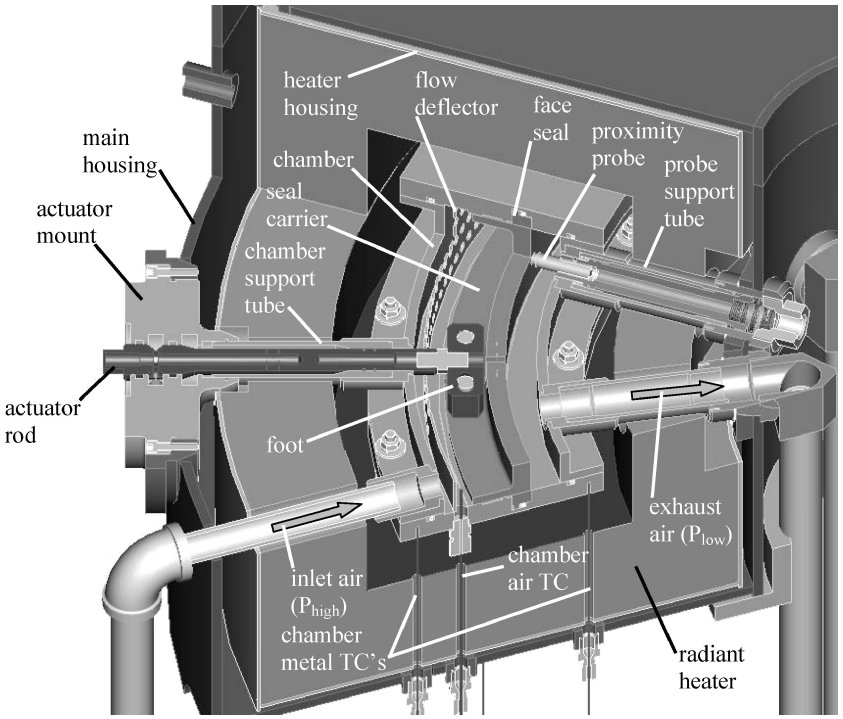

Fig. 7 Rig cutaway detail.

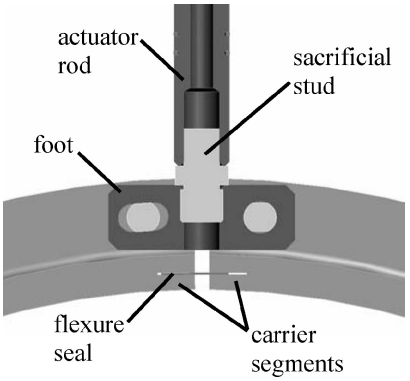

Fig. 8 Actuator rod foot-carrier detail.

Seal Carrier Design

The seal carrier assembly is made of nine segments that are joined together by pinned connections to the actuator rod feet. Figure 9 shows two of these segments assembled with an actuator rod. These structures not only support the seal segments that would exist in an actual engine, but they must also support the cooling/purge air pressure load that exists along the seal carrier backside, as well as the pin reaction loads at the carrier's ends. These loads occur inside the chamber at the highest temperatures. The carriers must also provide for secondary sealing along the chamber upper and lower lid structures, as well as between the carrier's own joint ends. In doing so, the carriers must maintain their shape to prevent nonuniform circumferential clearance distribution (out of roundness) of the seal segments.

The nine carrier segments are made of Inconel 718. This material was selected for its high-temperature strength and creep properties and is widely used for turbine engine hot section components. The carriers have a U-shape cross section to provide a rigid structure with reduced mass. They have an inner radius of 10.25 in. (260.35 mm), a width of 2.0 in. (50.8 mm), and a span of about 40 deg. The side flanges are 0.25 in. (6.35 mm) thick. The sections of these parts have been overdesigned to prevent displacement due to pressure and thermal loading. The authors recognize that the carrier segments, as well as other components, will need to be optimized to reduce weight for actual engine applications. Selecting optimal section designs is left for future exercises. seal carrier

Actuator Rod Assembly

The actuator rod assembly is shown in Figs. 7–9. The assembly is made of three major components, namely, the actuator rod, the sacrificial stud, and the foot, all made of Inconel 718. The actuator rod assembly functions as the link between the carrier segments and the actuators. Because the carrier segments are always pressure loaded, the rods and actuator load trains remain in tension. This mitigates backlash effects on positional accuracy. The rods act to position the carriers in the radial and circumferential directions and are supported by the chamber support tubes.

The actuator rods have an enlarged diameter on the end that bears against the actuator mount. Tight radial clearances [0.0015 in. (0.038 mm)] at this location serve to align the actuator rods. Toward the foot end of the actuator rod is a series of metal piston ring seals. The ring seals act to seal the chamber air, as well as to provide a bearing surface against the support tubes for alignment. The actuator rod is connected to the foot through a stud to provide a sacrificial part in case the connecting threads bind due to oxidation, preventing disassembly of the rod and foot. A high-temperature solid lubricant will be used on the threads to help prevent binding.

Seal Carrier Movement

Because the carriers are constrained by a pinned connection at one end and a slotted connection at the other, the segments must shift circumferentially as they are displaced in the radial direction. The slots in the feet are cut on a tangent to the radius on which the carrier pinholes are located. This keeps the carrier segments from cocking (ends of the carrier segment kept at the same radius) while they are displaced in both the radial and circumferential directions. The circumferential length of the carrier segments, as well as the length of the slot in the actuator rod foot, allows a radial displacement of 0.2 in. (5.1 mm) for each of the nine segments. The slots for the flexure seals have adequate clearance to prevent the segments from becoming arch bound as the segments are moved radially inward.

The pins are made of Inconel X750. This material was chosen for its high strength and creep resistance at high temperatures, as well as its wear resistance to other nickel-based alloys.[10] In particular, the material was selected to help minimize galling against adjacent Inconel 718 components. The pins have flats machined on the diameter that contacts the slots. This provides a bearing surface and lowers the contact stress developed between the pin and foot. The pins are designed with a slip fit for ease of assembly.

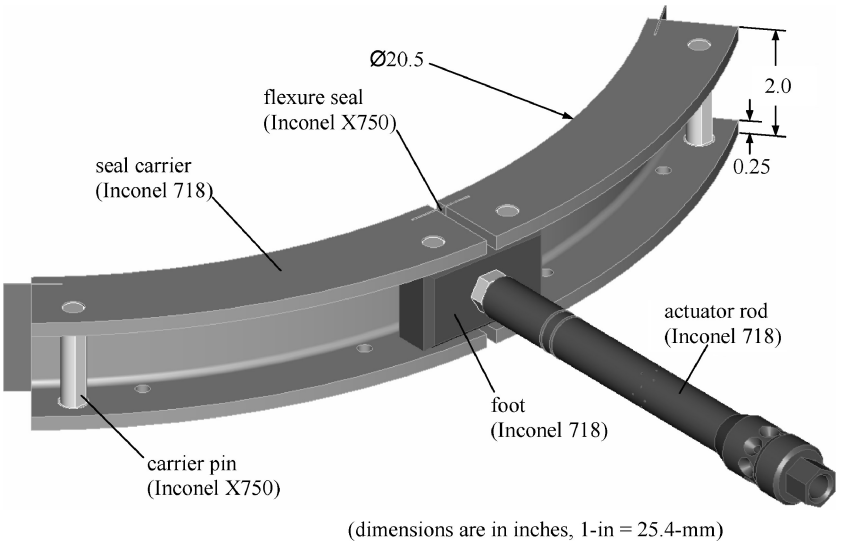

Fig. 9 Seal carrier and actuator rod assembly.

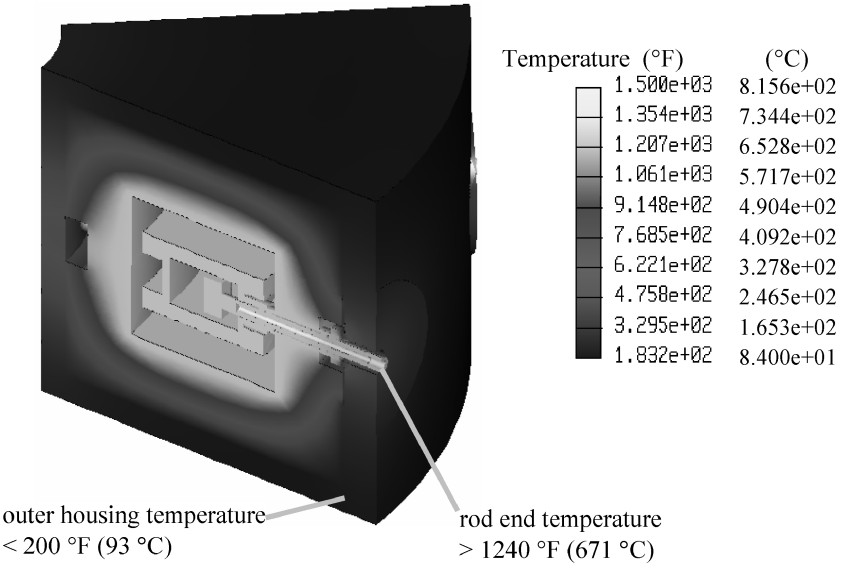

Fig. 10 Assembly thermal analysis (no rod cooling).

Actuator Rod Thermal Design

Figure 10 shows the results of a thermal analysis on the rig assembly with the chamber temperature of 1500°F (816°C). The model contained the stainless steel housing, the ceramic fiber radiant heater, and the Inconel 718 chamber and actuator rod assembly. All component surfaces inside the radiant heater (including the radiant heater surface) were set to 1500°F (816°C). A convection coefficient of 4.4 Btu/ft$^2 \cdot$h$\cdot$°F (25 W/m$^2 \cdot$K) was applied to the outer housing surfaces to represent free convection of air at ambient conditions. A steady-state thermal analysis estimated the rod-end temperature at 1240°F (671°C). This rod-end temperature greatly exceeds the upper operating temperature [~250°F (121°C)] allowed by conventional hydraulic actuators. A cooling scheme for the rod end was then designed to allow the use of conventional actuators. The cooling scheme, shown in Fig. 11, allows the actuator rod and support tube to function as a tube-in-tube heat exchanger using a small flow rate of ambient [70°F (21°C)] air to cool the assembly.

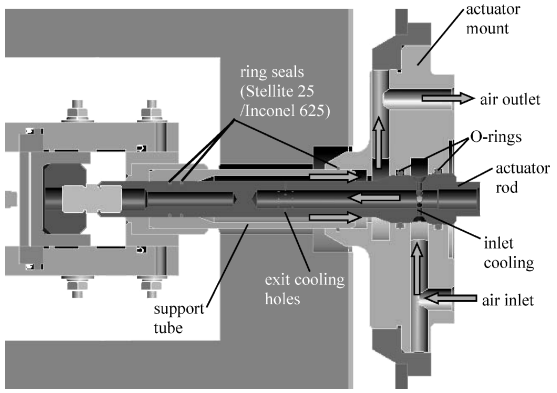

Fig. 11 Cooled actuator rod design.

Heat Transfer Analyses

The authors performed a simple one-dimensional heat transfer analysis to determine the feasibility of the cooling scheme by bounding the required flow rate. In this analysis, the heat conducted down the slender actuator rod [Eq. (2)] is balanced by the heat that is carried away by the cooling air [Eq. (3)] (see Ref. 11):

$$q_{\text{cond}} = \frac{kA}{L(T_h - T_c)} \tag{2}$$

$$q_{\text{conv}} = \dot{m} C_p (T_0 - T_i) \tag{3}$$

Based on the low flow rates that were calculated, the authors implemented the features of the cooling scheme to the rod assembly

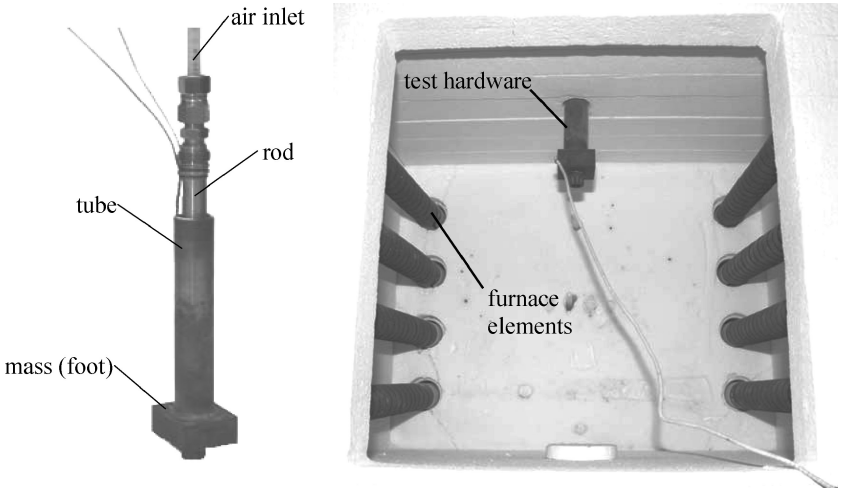

Fig. 12 Cooled rod test hardware and furnace assembly.

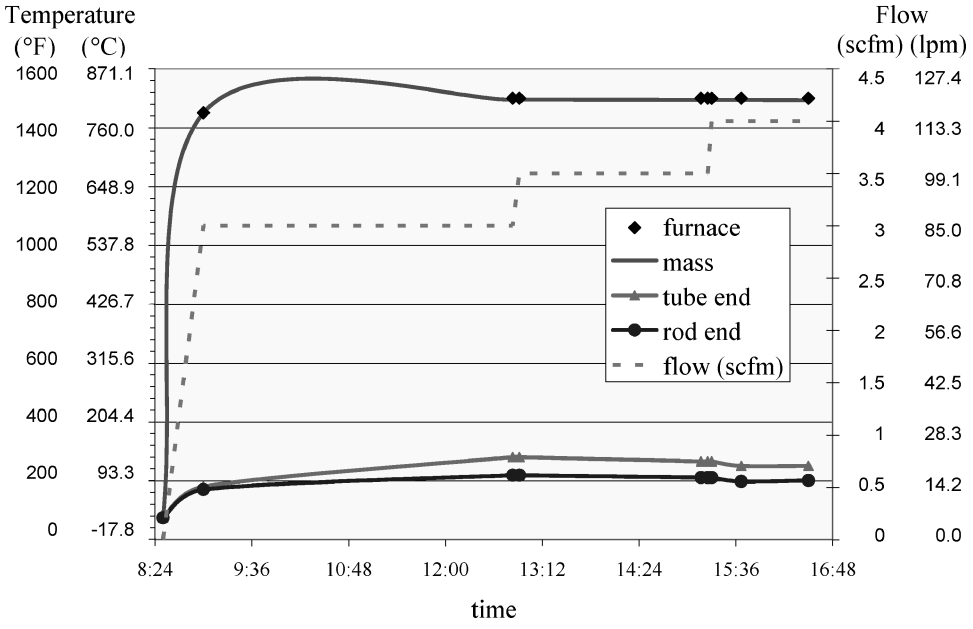

Fig. 13 Cooled rod experimental results.

shown in Fig. 11. The cooling holes were made from three sets of six, 0.03-in. (0.76 mm-) diam holes drilled around the circumference of the hollow rod. Ambient air, supplied at the rod end through features in the actuator mount, travels axially through the center of the rod, passes radially through the cooling holes, and exits between the support tube and outer diameter of the rod.

Experimental Validation

A mock-up of the cooled actuator rod design was built to validate the calculations (Fig. 12). A solid steel block (simulating the actuator foot) was bolted to one end of a stainless-steel tube (simulating the rod). Another larger tube was welded to the block (simulating the support tube) in a concentric arrangement. An air supply line was attached to the end of the inner tube from which the assembly was supported and inserted into a box furnace as shown in Fig. 12. The insulation thickness of the furnace closely approximated that of the radiant heater designed for the rig. A plastic supply line was used minimize heat loss through the supply tube.

Thermocouples were attached to measure the temperatures of the mass, the end of the inner rod, and the end of the outer tube. The furnace was heated to 1500°F (816°C) and, after the mass temperature stabilized at 1500°F (816°C), ambient air at approximately 70°F (21°C) was supplied to the assembly. Figure 13 shows the results of the furnace test. Temperatures of the furnace, mass, tube end, and rod end are shown as a function of time on the left vertical axis. The cooling air volumetric flow is shown on the right vertical axis. Figure 13 shows that, for minimal airflow [3.0–4.0 scfm (85–113 lpm)], both the tube and rod end temperatures were kept below 250°F (121°C). Thus, the cooling scheme design was successfully validated and implemented into the rig design to allow the use of conventional actuators. Careful attention was paid to this cooled actuator rod design to lay the groundwork for an approach scalable to an engine application.

Actuator Rod Stress Analysis

The chamber pressure on the outer surfaces of the carriers creates a tensile load on the actuator rods. Additional tensile loading comes from the frictional drag of the face seals that contact the sides of carrier segments. The actuator rods were sized to handle a 3000 lbf (13.3 kN) tensile load due to the chamber pressure, face seal drag, and a 1.5 factor of safety. Because one end of the rod operates in the high-temperature zone, the thin sections of the hollow rod where the piston ring seals are seated were a concern for stress concentration. A structural analysis on the rod design under a 3000-lbf (13.3-kN)

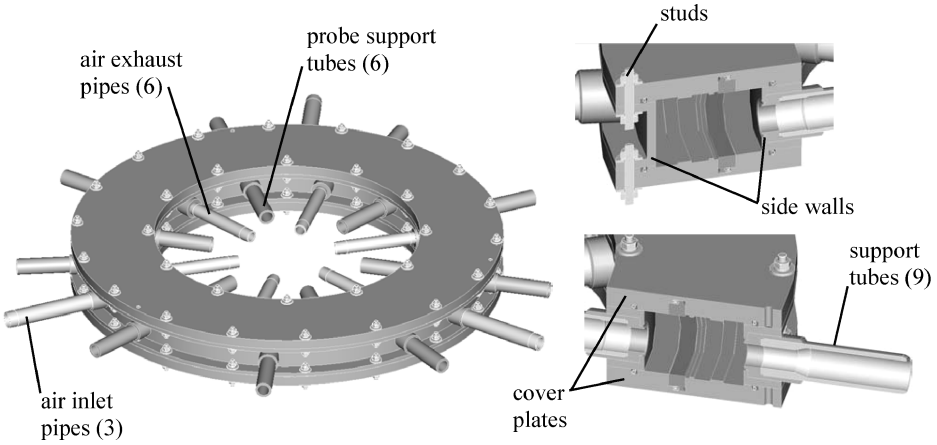

Fig. 14 Chamber assembly.

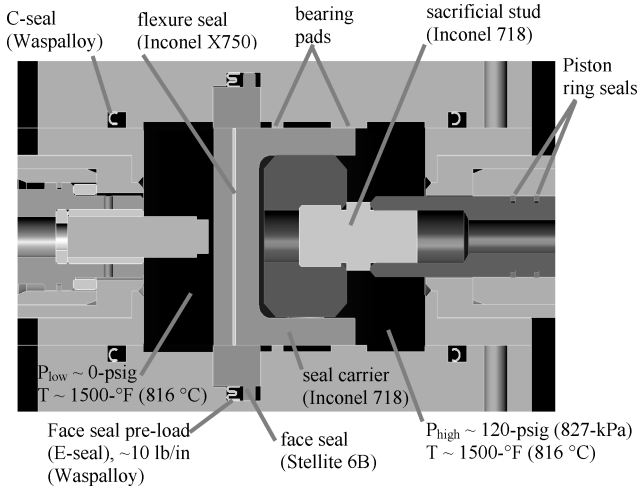

Fig. 15 Chamber detail and seal locations.

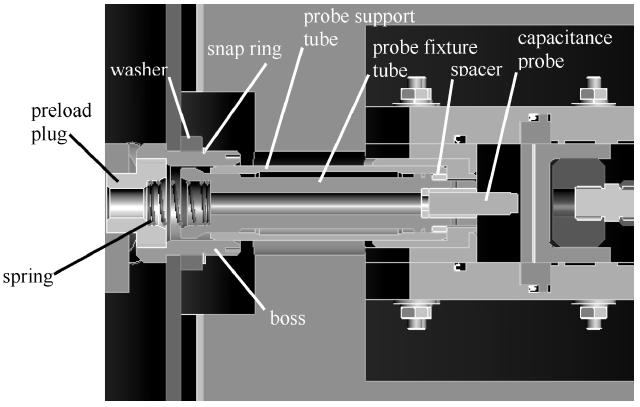

Fig. 16 Proximity probe fixture assembly.

tensile load at 1500°F (816°C) showed that the stresses were kept well below the maximum of 15 ksi (103 MPa) to ensure a minimum life of 300 h at these maximum conditions.

Chamber Design

The chamber assembly, shown in Fig. 14, serves as a pressure vessel, support, and alignment structure for the carrier–actuator rod assembly. In doing so, it is the most critical static structure of the entire rig. The Inconel 718 chamber is formed from two bands that make up the sides of a rectangular annulus and two rims that form the upper and lower cover plates. The bands are formed from two 0.375-in.- (9.525-mm.) thick, rectangular plates that are rolled and welded at their respective ends. The annulus formed from this assembly has an outer diameter of 25 in. (635 mm), inner diameter of 19 in. (482.6 mm), and a height of 2 in. (50.8 mm). The upper and lower cover plates are fixed to the side walls via stud and nut assemblies (Inconel 718). The studs are used for ease of disassembly in case the stud threads bind with their nuts due to oxidation. The same compound used on the actuator rod assembly will be utilized to prevent binding of the fasteners due to thermal cycling.

Figure 15 shows a detailed view of the chamber cross section. Aside from a number of metallic seals that will be discussed in a later section, Fig. 15 shows that the upper and lower cover plates contain bearing pads to prevent the carrier segments from cocking as they are radially displaced. The carrier segments will operate between the cover plate bearing pads with a 0.006-in. (0.152-mm) total clearance.

A series of tubes protrude from outer and inner sides of the chamber in the radial direction. Bosses that are welded to the sidewalls of the chamber support the tubes. The tubes are fixed to the bosses via press-fit or threaded arrangements, depending on their function. The tubes that are used for support, alignment, and air exhaust are press fit into the bosses, whereas the tubes that are face seal used to supply/exhaust air to/from the chamber are threaded into the bosses. A standard boss design was used for ease of manufacturing.

Support Tubes

Nine tubes that are equally spaced provide support and alignment for the entire chamber assembly. The support tubes are made of Inconel 718 and have outer and inner diameters of 1.25 in. (31.75 mm) and 1.0 in. (25.4 mm), respectively. The inner diameter necks down to 0.75 in. (19 mm) to provide alignment and support to the actuator rod ends as shown in Fig. 11.

Probe Support and Air Exhaust Tubes

There are 12 common tubes assembled around the inner chamber wall. These tubes, also made of Inconel 718, provide support for the proximity probe fixtures, as well as for exhaust ports that allow the air that leaks past the carrier segments to be vented out of the rig. A common tube design was used to allow interchanging of exhaust ports and instrumentation depending on research needs, as well as for ease of manufacturing.

Proximity Probe Fixture

The proximity probes are held at a constant standoff to the chamber inner wall via a spring-loaded piston arrangement as shown in Fig. 16. The sensor is held inside the end of a probe fixture tube via a split bushing and two set screws. The fixture tube houses a metal ring seal that blocks the air leaking past the carrier assembly from passing between the fixture tube and the probe support tube. A spring is engaged between the fixture tube end and a plug

that is threaded into a boss that is clamped to the inner housing cylinder via a snap ring and washer arrangement. The spring forces the shoulder of the fixture tube against a spacer seated inside the boss. The spring-loaded mounting keeps the proximity sensor at a relatively constant position to the chamber inner sidewall during the initial heating of the rig. This arrangement also allows for easy removal of the probes without the need to dismantle the housing.

Chamber Structural Analysis

The chamber walls, cover plates, and supporting structures were designed to maintain their maximum stresses below 15 ksi (103 MPa) to ensure a minimum life of 300 h under the maximum conditions of 120 psi (827.4 MPa) and 1500°F (816°C). In particular, the cover plate was designed to minimize deflection, ensuring that the assembly maintained adequate preload on the face seal. Figure 17 shows the stress and displacement results from a structural analysis of the cover plate. This conservative analysis included a 120-psi pressure load across the entire plate at 1500°F (816°C), along with the C-seal and E-seal compression loads of 300 lbf/in. (52.5 N/mm) and 10 lbf/in. (17.5 N/mm), respectively. Figure 17 shows that maximum deflection occurs at the E-seal groove, as would be expected due to the reduced thickness of the section. The maximum deflection [∼0.004 in. (0.109 mm)] is well below the E-seal compression of 0.015 in. (0.38 mm). Maximum stresses are shown to be below the 15-ksi (103-MPa) design limit, except around the bolt-hole regions. The higher stresses along these regions are believed to be an artifact of the constraints applied to the bolt holes and are believed not to be of concern.

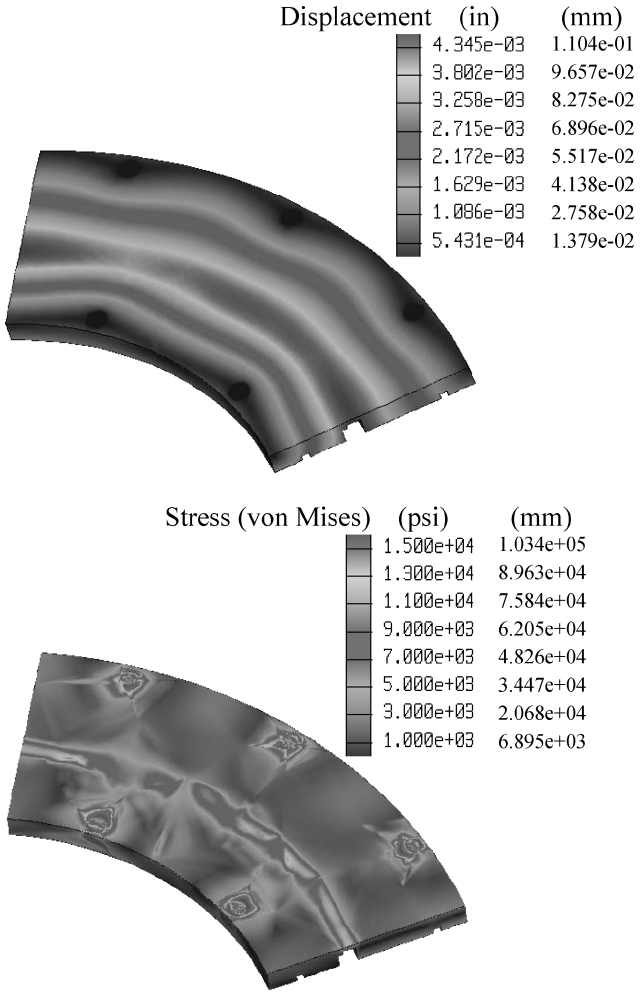

Fig. 17 Chamber cover plate structural analysis results.

Seals

Although the shroud seals for the ACC system are not being utilized in the test rig, there are a number of secondary seals required due to the nature of the ACC system and rig designs.

Flexure Seals

Flexure seals, shown in Figs. 8 and 9, are used to prevent the radial flow of pressurized air between the carrier segment joints. The 2.0-in.- (50.8-mm-) wide by 0.9-in.- (22.9-mm-) long flexures are made of 0.02-in. (0.51-mm) Inconel X750 sheet stock. This material was again chosen for its galling resistance to the carrier material. The carrier slits that contain the flexures are designed with a 0.01-in. (0.25-mm) clearance. The seals use the pressurized air to seat themselves, sealing on the lower slit surface of the carriers. The slit in one carrier segment is parallel to the slit of the adjoining carrier segment, making the flexure seal surface normal to the radial flow. The angles of the slits vary no more than 0.5 deg over the 0.2-in. (5.08-mm) stroke of the carrier segments. The bending stress in the flexures [∼10 ksi (69-MPa)] created by a 120-psig (827-kPa) pressure load is well below the 15-ksi (103-MPa) limit.

Flange Seals

The chamber contains four C-seals, two on the upper and lower outer diameter flanges and two on the upper and lower inner diameter flanges of the cover plates, as shown in Fig. 15. The seals are made of Waspalloy and have a cross-sectional thickness of 0.02-in. (0.51-mm). The seals were designed by Perkin–Elmer Fluid Sciences (Beltsville, Maryland) to seal against a 120-psi (827-kPa) pressure at 1500°F (816°C), and they require a 300-lbf/in (52.5-N/mm) seating load per seal at assembly. Waspalloy has excellent high-temperature strength and creep resistant properties, as well as good wear resistance to nickel-based alloys.

Face Seals

The upper and lower cover plates also house a metal face seal assembly, shown in Fig. 15. These seals act to block the pressurized air from flowing between the cover plates and carrier segments. The face seal, made of Stellite 6B, is a pressure balanced design and utilizes an E-seal as a preload and secondary seal device. Stellite 6B was selected for the face seal material due to its high-temperature properties and antigalling performance against Inconel 718. The E-seals, also designed by Perkin–Elmer Fluid Sciences and made of Waspalloy, provide a closing force to the face seal on the carrier segments and prevent air from leaking between the face seal and cover plate. Each E-seal provides about 10-lbf/in. (17.5-N/mm) preload to its corresponding face seal. The face seal was designed with a generous cross section, due to its large diameter, to provide stiffness for operation as well as manufacturing. Future studies will investigate alternate face seal designs based on the performance of the current design. The sealing surface of the face seals is to be manufactured with an 8-rms finish and a flatness of 0.0003 in. (0.008 mm). The carrier segments are to be finish ground as an assembly with the flexure seals in place. The outer sides of the carrier assembly are to be held to an 8-rms finish, a flatness of 0.0003 in. (0.008 mm), and parallel to 0.0005 in. (0.013 mm).

Ring Seals

The actuator rod contains two pairs of expanding concentric ring seal sets on its bearing surface as shown in Fig. 11. Each pair is made of an outer Stellite 25 ring and an inner Inconel 625 ring. The outer ring has a rectangular cross section [approximately 0.022 in. (0.56 mm) high by 0.05 in. (1.27 mm) wide] with a step cut gap configuration (lap joint) and a gauge gap of approximately 0.025 in. (0.64 mm). The inner ring has a rectangular cross section [approximately 0.02 in. (0.51 mm) high by 0.05 in. (1.27 mm) wide] with a square cut gap configuration (butt joint) and a gauge gap of approximately 0.045 in. (1.14 mm). The seals were designed by Precision Rings, Inc. (Indianapolis, Indiana), for 120 psi (827 kPa) at 1500°F (816°C).

Table 1 Seal leakage

	Pressure drop		Temperature		Flow	
Location	psi	kPa	°F	°C	scfm	lpm
C-seal	120	827	1500	816	1.6	45.3
Ring	120	827	1500	816	0.6	17.0
Flexure	120	827	1500	816	23.3	659.8
Face	120	827	1500	816	2.1	59.5
E-seals	120	827	1500	816	5.4	152.9
Total	——	——	——	——	33.1	937.3

Seal Leakage

Figure 15 shows the main seal locations and, hence, leakage paths, of the chamber and carrier assemblies. The main locations of concern are between the sides of the carriers and the chamber cover plates, the chamber outer flange, between the joints of the carriers, and along the actuator rods. As discussed earlier, most of the seals were of a standard design (metal ring seals, C-seals, E-seals). The leakages of these seals were provided by the corresponding manufacturer, based on the conditions specified. The face and flexure seals, however, were designed by the authors, and their leakages had to be calculated. The details of the steps taken and equations used for those procedures are provided in the Appendix. The approaches are summarized hereafter. The leakage results, either provided by the seal manufacturer or estimated by the authors, are given in Table 1.

Face Seal

Because of the moderate pressure drop across the face, calculation of the leakage between the face seal and carrier surfaces required the authors to determine whether the flow was choked or not. The procedure involved an iterative process using the equations of one-dimensional, radial, adiabatic flow between two parallel.[12] An inlet Mach number was iterated for such that choked conditions were achieved at the outlet. The outlet pressure was then compared to ambient to verify if choking actually occurred. Using this procedure, the authors found that the flow was not choked anywhere along the flowpath and that the leakage across the face was approximately 1.0 scfm (28.3 lpm) per seal.

Flexure Seals

The authors estimated a worst-case scenario for the flexure seal leakage and assumed choked flow through the clearance area between the carrier slots and the flexures. Calculating the flow in this manner provided an upper bound on the leakage through the carrier segment joints. The authors assumed a seated clearance between the carrier slots and the flexures of 0.0005 in. (0.0127 mm). This clearance gives an area of 0.001 in.^{2} (0.645 mm^2), with the carrier width at 2.0 in. (50.8 mm) per flexure seal. Equation (4) gives a relation for the maximum mass flow of air through an area under choked conditions[13]:

$$\dot{m}_{\max} = 0.6847\left(p_\circ A^* \Big/ \sqrt{RT_0}\right) \tag{4}$$

The choked flow assumption produced a total flow of 23.3 scfm (659.8 lpm) as shown in Table 1.

Heating Systems

The test rig utilizes two heating systems to simulate the thermal environment of the shroud seal backsides that are cooled at 1200–1300°F (649–704°C) in an actual turbine engine.

Radiant Heater Design

The radiant heater is formed from two halves (U-shaped in cross section) that enclose the chamber in a rectangular annulus as shown in Fig. 7. The body of the heater is made of a lightweight alumina–silica fiber composition. The heating elements, made of an iron–chrome–aluminum composition, are embedded under the annular surface in a flat sinuated pattern. The ceramic fiber body has a density and thermal conductivity of approximately 0.15 lbm/ft^3 (2.4 kg/m^3) and 0.1 Btu/h · ft · °F (0.18 W/m · K) at 1500°F (816°C), respectively. Each radiant heater will be contained in a housing made of 0.062-in.- (1.575-mm-) thick stainless-steel sheet. The housings will provide molds for the ceramic fiber bodies during manufacturing and a protective shell for assembly into and out of the rig. Porcelain bushings isolate the heating element power leads from the heater and main housings.

Element Zones

The heating elements for both the upper and lower halves of the heater are to be wired in six separate circumferential zones. Each zone from the lower half will be wired in parallel to its corresponding zone in the upper half such that each circumferential zone (upper and lower) will be powered through one controller. This will give researchers the ability to heat the chamber in a nonuniform fashion, simulating the phenomenon that can occur in an actual engine, where shroud seal backside temperatures can vary by 150°F (66°C) from the 12 to 6 o-clock positions.

Air Heater System

The purpose of the air heater is to allow pressurization of the chamber and, hence, pressure loading of the carrier assembly, in a relatively isothermal environment. Because the seals described in earlier sections are not air tight, leakage past the carrier assembly and actuators rods will occur. Whereas the leakage was calculated to be relatively small [∼30 scfm (850 lpm)], large temperature variations between hot section components and the pressurized air can cause thermal distortions of the components at the leakage locations. To mitigate nonuniform thermal distortion of components, the authors sized an air heating system to minimize the temperature difference between the pressurized air and the radiant heater, and used a baffle to deflect the airflow in a uniform fashion around the chamber annulus. Although the authors did not expect to have to supply a large amount of flow to the rig, providing even low flow rates [below 100 scfm (2832 lpm)] of heated air at 1500°F (816°C) and 120 psi (827 kPa) can be challenging.

Heater Design

The heater was designed to supply up to 80 scfm (2265 lpm) of air at 120 psi (827 kPa) and 1500°F (816°C). The heater is made of two 36-kW, in-line, flanged heaters, manufactured by Osram Sylvania (Danvers, Massachusetts) that are used in series to achieve the 1500°F (816°C) temperature specification. Each heater is composed of six heating elements housed in a 304 stainless-steel schedule 80 pipe that has 300-lbf (1.3-kN) welded flanges on either end. The elements are wired such that each pair is on one phase of the three-phase power supply. Air, supplied to the housing, flows through cylinders that enclose the individual heating elements that line the inner diameter of the housing. The heaters are supplied with thermocouples to measure element temperature and the process air temperature at the exit of the housing to prevent element burnout.

Housing

The housing shown in Fig. 5 is made of 304 stainless steel. The housing is made of two concentric cylinders that make up the annular walls, a base plate, and a lid. The annular cross section dimensions of the enclosed housing are 13.5 in. (343 mm) wide by 12 in. (305 mm) high. Each cylinder is made of 0.25-in. (6.35-mm) plate that is rolled and welded together. The inner cylinder has an inside diameter of 9 in. (229 mm), whereas the outer cylinder has an outer diameter of 37 in. (940 mm). The cylinders are welded to the base plate that forms the main housing. Stainless-steel bosses, 7.5 in. (190.5 mm) in diameter, are welded to the outer annular wall of the housing to support the actuator mounts. The bosses provide adequate depth of section through which the actuator mounts are bolted. The bosses also serve to make the rig design modular, in that different actuator mounts and actuators can be plugged into the rig and tested. The base plate contains pressure vent ports in case the chamber should leak, such that the housing will never become a pressure vessel. The main housing outer wall and lid contain lifting eyes for transporting the entire assembly.

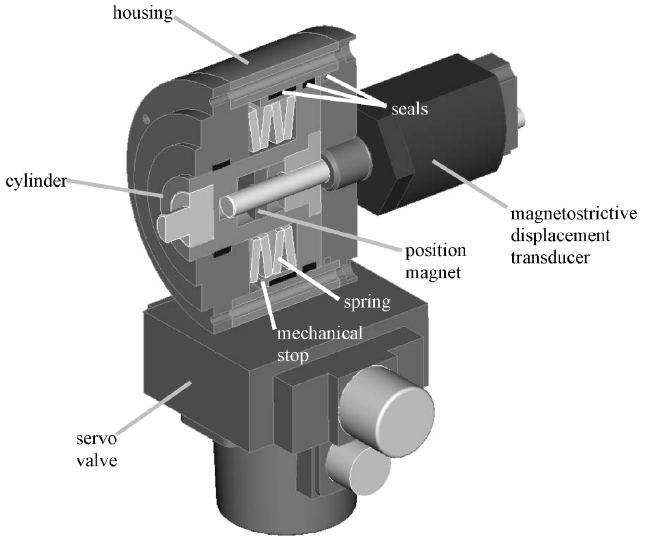

Fig. 18 Custom actuator design.

Actuator Mounts

The actuator mounts provide supporting and aligning structures for the actuators and the actuator rods, as well as inlet and exhaust ports for the actuator rod cooling air (Fig. 11). The actuator mount's inner diameter provides an aligning and bearing surface for the actuator rod end. Each mount contains a metal ring seal to prevent exhaust cooling air from flowing into the radiant heater and two high-temperature elastomeric O-rings that prevent the inlet cooling air from flowing along the outer surface of the actuator rod.

Customized Hydraulic Actuator

The authors are currently designing a low-profile, servo-controlled, hydraulic actuator. Industrial hydraulic actuators, which met the specified load, stroke, response, and accuracy requirements, were found to occupy too much space for flight hardware. The authors decided to design a custom actuator using standard components of current, high-accuracy, and robust hydraulic actuator systems.

Actuator Design

The present hydraulic actuator design is shown in Fig. 18. The actuator comprises a cylinder section, servo valve, and position sensor. The cylinder is constructed with low-friction and high-temperature seals for minimal hysteresis. The actuator cylinder works against a mechanical spring load so that the ACC system would fail to open in the event of hydraulic pressure loss. Mechanical stops are included to prevent overtravel of the carrier segments. The servo valve is a digital control with internal feedback for positional accuracy.

The system is designed for a 0.20-in. (5.08-mm) stroke with a velocity of 0.04 in./s (1.02 mm/s) and a 3-in. (76-mm) bore piston. The actuator occupies a length of about 6.5 in. (165 mm). One-half of the length comes from a commercially available displacement transducer that runs inline with the cylinder centerline. This length could be further reduced using a custom designed transducer.

Accuracy

The servo system has a 0.0003-in. (0.0076-mm) positional accuracy with full velocity and acceleration profile capabilities. The displacement transducer employs magnetostrictive technology with digital output and is capable of a 0.00008-in. (0.002-mm) resolution. Coupled with the capacitance-based probes and the hardware tolerance specifications, the actuator will have positioning capabilities of 0.001 in. (0.025 mm) under full load.

Instrumentation

The test rig is equipped with a great deal of instrumentation. Measurements of displacement, temperature, pressure, and flow rate will provide researchers with necessary data for evaluation of actuator concepts, monitoring environmental conditions of the rig, feedback control for rig operation, and health monitoring of the rig and support systems.

Capacitance Sensors

High-temperature capacitance-based proximity probes (manufactured by Capacitec of Ayer, Massachusetts) will be utilized to measure the displacement rate and position of the carrier segments, as shown in Figs. 7 and 16. Four probes will be positioned such that three are equally spaced at 120 deg, whereas two probes are positioned 180 deg apart. The probe positioning will allow the measurement of an effective and true shroud diameter. The probes will target the ends and midpoints of various carrier segments to evaluate the positioning accuracy and repeatability of the independent actuators. The probes chosen for this work have a body diameter of 0.375 in. (9.52 mm) and length of 1.5 in. (38.1 mm). The probes have a linear range of 0.100 in. (2.54 mm), an accuracy of $1.0E-5$ in. ($2.54E-4$ mm), a resolution of $1.0E-7$ in. ($2.54E-6$ mm), and can function in environments up to 1832°F (1000°C). The signal amplifiers have a frequency response of 15 kHz. The probes were calibrated by the manufacturer at various temperatures ranging from 300 to 1500°F (149–816°C). The test rig is designed to permit the evaluation of other displacement probes currently under development.

Temperature

Temperature measurements will be utilized to quantify the thermal environment in which components will be evaluated, to control the air and radiant heater systems, and for health monitoring of various components. A standard thermocouple design of a type-K, grounded bead with a 0.063-in.- (1.6-mm-) diam, 12-in.- (305-mm-) long sheath (Inconel 600) will be utilized throughout the rig. All thermocouples that protrude the main housing will be fixed to the housing base or lid via compression fittings. The chamber air temperatures will be measured at three circumferential locations on the high-pressure side of the carriers. Two thermocouples will be positioned near two of three chamber air inlets, and one will be positioned between two air inlets. These thermocouples will show how well the pressurized air is mixed by the chamber baffle.

The chamber flange metal temperatures will be measured via two surface thermocouples attached to the inner and outer flange on the lower cover plate. These thermocouples will straddle one of the air thermocouples as shown in Fig. 7. One of the nine actuator rod ends will have a thermocouple to monitor the rod cooling system and will determine how much pressure should be used for the cooling air supply.

Pressure

Pressure of the inlet air to the chamber will be measured via pressure transducers off of the air inlet pipes before entering the rig with static pressure taps. This will provide the high-side chamber pressure. Pressure will also be measured off of the exhaust pipes to ensure that no backpressure exists in the chamber vent.

Flow

The inlet air mass flow will be measured with a flow meter before it enters the air heater. This flow will indicate the chamber air leakage and, hence, health of the secondary seals. This measurement will be particularly important for the life of the face and flexure seals, in that they are in the most challenging environments with regard to temperature, pressure, and displacement.

Conclusions

The design of a first-generation, hydraulically powered mechanical system to provide active clearance control for turbine blade tip shroud seals, along with a test rig to evaluate its response and positioning accuracy, has been presented. The system employs a segmented seal carrier structure, independent hydraulic actuators,

high-temperature proximity probes, and feedback control. The ACC system has been designed to position the carrier segments and, hence, clearance of the shroud seal accurately, to within 0.004 in. (0.102 mm) or less. The ACC system and test rig have been designed to function at pressures up to 120 psi (827 kPa) and temperatures up to 1500°F (816°C) with a minimum cycle life of 300 h at these maximum conditions.

The ACC system developed in this work will be evaluated in the described test rig under a series of temperature and pressure conditions to evaluate its performance in a simulated turbine environment. The results of this testing will be used to further develop the current actuator design, as well as other actuator concepts. ACC system components will be optimized to increase cycle life while reducing weight for future flight hardware development.

Appendix: Face Seal Leakage Analysis

An entrance Mach number (M_1) was assumed, from which the inlet temperature, flow velocity, Reynolds number, and friction factor are calculated with Eqs. (A1–A4), respectively:

$$T_1 = T_i \Big/ \left[1 + (\gamma - 1)M_1^2 \Big/ 2C_L^2\right] \tag{A1}$$

$$M = u \Big/ \sqrt{\lambda RT} \tag{A2}$$

$$Re = 2\rho uh/\mu \tag{A3}$$

$$f' = k/Re^n \tag{A4}$$

where for laminar flow ($Re < 2300$), $k = 24$, and $n = 1$, and for turbulent flow ($Re > 3000$), $k = 0.79$ and $n = 0.25$.

The inlet pressure p_1 is found from Eq. (A5) based on a loss coefficient C_L (Ref. 14). The outlet Mach number M_2 is found via integration of Eq. (A6), which, with the assumption of a constant gap, gives the relation shown by Eq. (A7):

$$p_1 = p_i \Big/ \left[1 + \frac{(\gamma - 1)M_1^2}{2C_L^2}\right]^{\gamma/(\gamma - 1)} \tag{A5}$$

where $C_L = 0.6$.

$$\frac{\mathrm{d}M^2}{\mathrm{d}r} = \left(f'M^2\gamma - \frac{\mathrm{d}h}{\mathrm{d}r}\right)\frac{2M^2\{1 + [(\gamma - 1)/2]M^2\}}{h(1 - M^2)} \tag{A6}$$

$$-\frac{1}{\gamma}\frac{1 - M^2}{M^2} - \frac{\gamma + 1}{2\gamma}\ln\left[\frac{\frac{1}{2}(\gamma + 1)M^2}{1 + \frac{1}{2}(\gamma - 1)M^2}\right]\Bigg|_{M_1}^{M_2} = \frac{2\Delta rf'}{h} \tag{A7}$$

This process is repeated until an inlet Mach number is found such that a choked condition exists at the outlet ($M_2 = 1.0$). The outlet pressure p_2 is then checked against the ambient pressure p_0 to determine if the flow is truly choked. This is the case if $p_2 > p_0$. If $p_2 < p_0$, then the flow is subcritical, and M_1 must be found such that $p_2 = p_0$. The outlet pressure is calculated using

$$p_2 = p_1\frac{M_1}{M_2}\left\{\frac{1 + [(\gamma - 1)/2]M_1^2}{1 + [(\gamma - 1)/2]M_2^2}\right\}^{\frac{1}{2}} \tag{A8}$$

Acknowledgments

The authors acknowledge the NASA Glenn Research Center Revolutionary Aeropropulsion Concepts Project for supporting this research. The authors also recognize Arthur H. Erker and Michael Hoychick of Analex Corporation (Cleveland, Ohio) and Richard A. Tashjian of QSS Group, Inc. (Cleveland, Ohio) for their efforts and support in the design and the detailing of the active clearance control system and test rig.

References

[1]Halila, E. E., Lenahan, D. T., and Thomas, T. T., "Energy Efficient Engine, High Pressure Turbine Test Hardware Detailed Design Report," NASA CR-167955, June, 1982.

[2]Lattime, S. B., and Steinetz, B. M., "Turbine Engine Clearance Control Systems: Current Practices and Future Directions," NASA TM-2002-211794, July, 2002.

[3]Wiseman, M. W., and Guo, T., "An Investigation of Life Extending Control Techniques for Gas Turbine Engines," *Proceedings of the American Control Conference*, IEEE Service Center, Piscataway, NJ, Vol. 5, 2001, pp. 3706, 3707.

[4]"Air Travel Emissions," *Climate*, Rocky Mountain Institute, Snowmass, CO, URL: http://www.rmi.org/sitepages/pid600.php [cited April, 2002].

[5]McNamara, S., "Emissions and Energy Usage," *ERA Fast Facts*, European Regions Airline Association, URL: http://www.eraa.org [cited 22 Sept. 2000].

[6]Olsson, W. J., and Martin, R. L., "B747/JT9D Flight Loads and Their Effect on Engine Running Clearances and Performance Deterioration; Nacelle Aerodynamic and Inertial Loads (NAIL)/JT9D Jet Engine Diagnostics Programs," NASA CR-165573, Feb. 1982.

[7]Martin, R. L., "Nacelle Aerodynamic and Inertial Loads (NAIL) Project, Test Report," NASA CR-165760, May 1981.

[8]*Electronic Code of Federal Regulations*, Title 14, Aeronautics and Space, Federal Aviation Administration, Department of Transportation, Part 33, Airworthiness Standards: Aircraft Engines, 33.73 Power or Thrust Response, Amdt. 33-1, 36 FR 5493, 24 March 1971, Chap. 1.

[9]Juvinall, R. C., "Engineering Considerations of Stress, Strain and Strength," *Creep and Creep Rupture*, 1st ed., McGraw–Hill, New York, 1967, pp. 416, 417.

[10]Laskowski, J. A., and Dellacorte, C., "Friction and Wear Characteristics of Candidate Foil Bearing Materials from 25°C to 800°C," *Lubrication Engineering*, Vol. 52, No. 8, 1996, pp. 605–612.

[11]Incropera, F. P., and Dewitt, D. P, "Introduction to Heat Transfer," *Physical Origins and Rate Equations*, 1st ed., Wiley, New York, 1985, pp. 5–8.

[12]LeBeck, A. O., "Principles and Design of Mechanical Face Seals," *Seal Interface Tribological Modeling*, 1st ed., Wiley, New York, 1991, pp. 133–138.

[13]White, F. M., "Fluid Mechanics," *Isentropic Flow with Area Changes*, 1st ed., McGraw–Hill, New York, 1979, pp. 529, 530.

[14]Zuk, J., "Analytical Study of Pressure Balancing in Gas Film Seals," *ASLE Transactions*, Vol. 17, No. 2, 1974, pp. 97–104.